Diffraction of a Gaussian beam from a periodic planar screen

Em. E. Kriezis, P. K. Pandelakis, and A. G. Papagiannakis

School of Electrical Engineering, Division of Telecommunications, Aristotle University of Thessaloniki, GR-54 006, Thessaloniki, Greece

Received November 2, 1992; revised manuscript received July 7, 1993; accepted August 25, 1993

The diffraction of electromagnetic radiation from one-dimensional planar transmittive screens illuminated by Gaussian-profile beams is examined. The incident Gaussian beam is expressed as a superposition of elementary plane waves that propagate along different directions, with the aid of the plane-wave spectrum technique based on Fourier optics. For each elementary plane wave, the diffracted field is obtained by applying the spectral domain method combined with the method of moments. Results for the cases of normal and oblique incidence are in agreement with theoretically expected properties of such planar screens and are found to be very sensitive to the aspect ratio γ (strip width to period). The diffracted beam is composed of distinct subbeams that propagate along specific directions. These directions coincide with the Floquet harmonics generated by an incident plane wave propagating along the same direction as the initial beam.

1. INTRODUCTION

The diffraction of electromagnetic radiation from periodic screens has received great attention, as it has an enormous number of applications in seemingly diverse areas like integrated optics, acousto-optics, holography, and spectroscopy. A broad field of diffraction applications includes beam shapers, multiplexers, polarizers, spectral filters, and waveguide couplers, as well as distributed feedback, modulation, and signal processing.[1]

The majority of published approaches assume that the incident electromagnetic radiation has the form of a plane monochromatic electromagnetic wave.[2–4]

There are also a limited number of papers that address the more realistic situation of an incident beam field, that is, a Gaussian beam. The diffraction of Gaussian-profile beams from gratings that are composed of periodically modulated media (media that exhibit a periodic variation of the refractive index) has been discussed in detail.[5–8] The diffraction of Hermite–Gaussian beams of arbitrary order from sinusoidal, perfectly conducting gratings has been investigated.[9] Also, diffraction from a sinusoidal reactance plane as well as spatial modifications of the diffracted beams has been treated.[10]

The screen under study is constructed of periodically placed strips that are infinitely long, infinitesimally thin, and perfectly conducting. Therefore electromagnetic radiation can be transmitted through this screen in constrast to the grating structure of Ref. 9. To the best of our knowledge, no research has been done on periodic planar transmittive screens illuminated by Gaussian-profile beams; hence this paper.

The plane-wave spectrum technique based on Fourier optics is used to express the incident Gaussian beam as a superposition of elementary plane waves that propagate along different directions. For each elementary plane wave, the diffracted field is obtained by the use of the spectral domain method combined with the method of moments.

Equiamplitude contour maps of the diffracted near-field intensity for several configurations are given as numerical illustrations in Section 3, and they are discussed in detail. Furthermore, far-field radiation patterns are presented.

2. ANALYTICAL FORMULATION

The periodic planar screen is composed of strips that are placed periodically along the x direction with period L_x. The strips are assumed to be infinitesimally thin and perfectly conducting (Fig. 1). The structure is uniform along the y direction. The incident radiation arrives with the form of a two-dimensional (2D) Gaussian beam that propagates along a direction within the x–y plane, and its electric-field intensity vector is polarized along the y axis (perpendicular or TE polarization).

The 2D Gaussian beam is expressed by the following relation[11] in the local coordinate system (x', y', z'):

$$E_{y'}^{\text{inc}}(x', z') = E_0^{\text{inc}} \frac{w_0'}{w(z')} \exp\left[-\frac{x'^2}{w^2(z')}\right] \exp\left[-\frac{jkx'^2}{2R(z')}\right] \times \exp\{-j[kz' - \tan^{-1}(z'/z_0')]\}, \quad (1)$$

where w_0' is the spot size at the beam waist (spot size at $z' = 0$), $k = 2\pi/\lambda$ is the wave number, λ is the wavelength, and $z_0' = \pi w_0'^2/\lambda$. The spot size, $w(z')$, and the radius of curvature, $R(z')$, of the phase front of the beam are

$$w(z') = w_0'\left[1 + \left(\frac{z'}{z_0'}\right)^2\right]^{1/2}, \qquad R(z') = z'\left[1 + \left(\frac{z_0'}{z'}\right)^2\right]. \quad (2)$$

In the $z' = 0$ plane:

$$E_{y'}^{\text{inc}}(x', 0) = E_0^{\text{inc}} \exp\left(-\frac{x'^2}{w_0'^2}\right). \quad (3)$$

The first step in expressing the electric field at any point as a sum of plane waves is to apply the Fourier trans-

0740-3232/94/020630-07$06.00

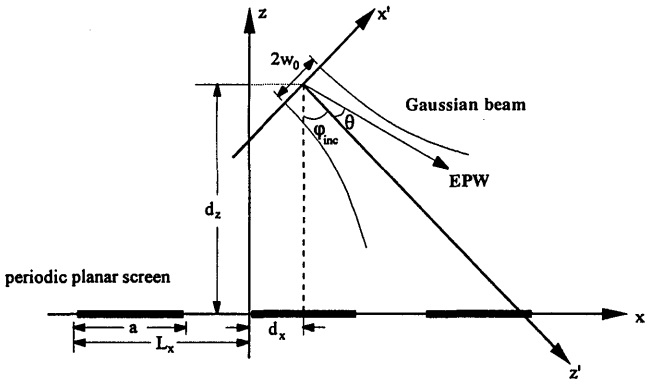

Fig. 1. Diffraction of a 2D Gaussian-profile beam from an array of conducting strips.

form to both sides of Eq. (3):

$$F[E_{y'}^{\text{inc}}(x',0)] = E_0^{\text{inc}}\sqrt{\pi}w_0' \exp(-\pi^2 w_0'^2 f_{x'}^2). \tag{4}$$

The electric field, $E_{y'}^{\text{inc}}(x',z')$, at any point is obtained by multiplying Eq. (4) by $\exp(j2\pi f_{z'}z')$ and taking the inverse Fourier transform[12,13]:

$$E_{y'}^{\text{inc}}(x',z') = E_0^{\text{inc}}\sqrt{\pi}w_0' \int_{-\infty}^{\infty} \exp(-\pi^2 w_0'^2 f_{x'}^2) \times \exp[j2\pi(f_{x'}x' + f_{z'}z')]\mathrm{d}f_{x'}. \tag{5}$$

If $\mathbf{f} = f_{x'}\hat{x}' + f_{z'}\hat{z}'$, and with $\mathbf{k}$ defined as $-2\pi\mathbf{f} = \mathbf{k} = \alpha'\hat{x}' + \beta'\hat{z}' = k(\sin\vartheta\hat{x}' + \cos\vartheta\hat{z}')$, where $|\mathbf{k}| = k$, Eq. (5) takes the form

$$\begin{aligned} E_{y'}^{\text{inc}}(x',z') &= \frac{E_0^{\text{inc}}w_0'}{2\sqrt{\pi}} \int_{-k}^{k} \exp\left(-\frac{w_0'^2\alpha'^2}{4}\right) \times \exp[-j(\alpha'x' + \beta'z')]\mathrm{d}\alpha' \\ &= \frac{E_0^{\text{inc}}kw_0'}{2\sqrt{\pi}} \int_{-\pi/2}^{\pi/2} \exp\left(-\frac{w_0'^2k^2\sin^2\vartheta}{4}\right) \times \exp[-jk(\sin\vartheta x' + \cos\vartheta z')]\cos\vartheta\mathrm{d}\vartheta. \end{aligned} \tag{6}$$

In Eq. (6) the limits of integration have been modified with respect to Eq. (5) to account only for the nonevanescent uniform plane waves.

This can be written in discrete elementary plane wave (EPW) spectrum form as

$$\begin{aligned} E_{y'}^{\text{inc}}(x',z') &\approx \frac{E_0^{\text{inc}}w_0'}{2\sqrt{\pi}} \sum_n \exp\left(-\frac{w_0'^2\alpha_n'^2}{4}\right) \times \exp[-j(\alpha_n'x' + \beta_n'z')]\Delta\alpha_n \\ &\approx \frac{E_0^{\text{inc}}kw_0'}{2\sqrt{\pi}} \sum_n \exp\left(-\frac{w_0'^2k^2\sin^2\vartheta_n}{4}\right) \times \exp[-jk(\sin\vartheta_n x' + \cos\vartheta_n z')]\cos\vartheta_n\Delta\vartheta_n. \end{aligned} \tag{7}$$

The EPW expansion of relation (7) can be achieved in a number of ways, according to the method used for approximating the integral in Eq. (6). In this paper the terms arising from applying a Gaussian quadrature scheme to Eq. (6) are used to extract the number of EPW's necessary to represent Eq. (6). The mean-square error introduced by the approximate discrete summation of relation (7) is discussed in Section 3.

Expressions that are valid in the (x', y', z') local coordinate system can readily be transformed to (x, y, z) through the transformations

$$x' = (x - d_x)\cos\varphi_{\text{inc}} + (z - d_z)\sin\varphi_{\text{inc}}, \tag{8a}$$

$$z' = (x - d_x)\sin\varphi_{\text{inc}} - (z - d_z)\cos\varphi_{\text{inc}}. \tag{8b}$$

When the Gaussian beam is decomposed into a set of EPW's in system (x, y, z), each EPW is treated separately. The diffraction of an EPW from a periodic planar screen is formulated by the spectral domain method.[2,13] We present only the salient points of the method, which is found to be very efficient in analyzing periodic screens having a period L_x of the same order of magnitude as the wavelength λ.

We focus our interest on the nth incident EPW. Its component along the y direction is written as

$$E_{y,n}^{\text{inc}}(x,z) = A_n(\alpha_n)\exp[-j(\alpha_n x - \beta_n z)], \qquad \beta_n = (k^2 - \alpha_n^2)^{1/2}. \tag{9}$$

The quantities $A_n(\alpha_n)$, α_n are directly related to the parameters of the Gaussian beam.

Because of the periodicity of the screen along the x direction,[14] the diffracted electric-field intensity is expressed by a Floquet series expansion:

$$E_{y,n}^{d,\text{I}}(x,z) = \sum_{m=-\infty}^{\infty} B_{nm}\exp[-j(\alpha_{nm}x + \beta_{nm}z)], \qquad z > 0, \tag{10a}$$

$$E_{y,n}^{d,\text{II}}(x,z) = \sum_{m=-\infty}^{\infty} C_{nm}\exp[-j(\alpha_{nm}x - \beta_{nm}z)], \qquad z < 0, \tag{10b}$$

$$\alpha_{nm} = \alpha_n + 2m\pi/L_x, \qquad \beta_{nm} = (k^2 - \alpha_{nm}^2)^{1/2}.$$

The superscript d stands for the diffracted field, whereas superscripts I and II refer to the half-spaces $z > 0$ and $z < 0$, respectively.

The continuity of the tangential electric field along $z = 0$ leads to the following relation:

$$B_{nm} + A_n\delta(m) = C_{nm}, \tag{11}$$

where $\delta(m) = 0\ \forall\ m \neq 0$ and $\delta(0) = 1$.

The total tangential electric field should also vanish on the metallic portions of the screen:

$$[E_{y,n}^{d,\text{I}}(x,z) + E_{y,n}^{\text{inc}}(x,z)]\big|_{\text{on strips}} = 0. \tag{12}$$

The magnetic field can readily be deduced from the electric field with Maxwell's equation:

$$\mathbf{H} = -\frac{1}{j\omega\mu}\nabla\times\mathbf{E}, \tag{13}$$

whereas the induced surface-current density is related to the magnetic field as

$$\mathbf{J} = \hat{z}\times[\mathbf{H}(z = 0^+) - \mathbf{H}(z = 0^-)]. \tag{14}$$

Evaluating the expression for $\mathbf{H}$ from Eqs. (10a), (10b), and (13), we can substitute the result into Eq. (14) and

obtain the expansion of **J** in the form

$$\mathbf{J}_n(x) = \hat{y} \sum_{m=-\infty}^{\infty} J_{y,nm} \exp(-j\alpha_{nm}x), \tag{15}$$

which is the surface-current density induced along the metallic strips by the nth EPW. The coefficients $J_{y,nm}$ by the use of Eq. (11), are evaluated to obtain

$$B_{nm} = \frac{-k^2}{2\omega\varepsilon} \frac{1}{(k^2 - \alpha_{nm}{}^2)^{1/2}} J_{y,nm}. \tag{16}$$

Finally, by substituting Eqs. (10a) and (10b) into Eq. (12) and using Eqs. (15) and (16), we obtain the electric-field equation:

$$-\frac{k^2}{2\omega\varepsilon} \sum_{m=-\infty}^{\infty} \frac{1}{(k^2 - \alpha_{nm})^{1/2}} J_{y,nm} \exp(-j\alpha_{nm}x) = -A_n \exp(-j\alpha_n x). \tag{17}$$

Electric-field Eq. (17), holds on the metallic portions of the screen and, because of periodicity, need only be enforced on a single cell (period) of the surface.

The surface current is expanded in terms of appropriate basis functions (i.e., waveguide modes of a parallel-plate waveguide)[14]:

$$\mathbf{J}_n(x) = \hat{y} \sum_p F_{np} \Psi_p(x). \tag{18}$$

The spectral coefficients, $J_{y,nm}$ of the surface current are immediately related to the basis functions as

$$J_{y,nm} = \sum_p F_{np} \Psi_{p,m}, \tag{19}$$

$$\Psi_{p,m} = \frac{1}{L_x} \int_{\text{strip}} \Psi_p(x) \exp(j\alpha_{nm}x) dx. \tag{20}$$

The remaining step is to solve the electric-field equation for the unknown current coefficients, F_{np}, that are involved into a linear system by the use of the method of moments. The linear system acquires the following form:

$$\sum_p F_{np} \left[\sum_{m=-\infty}^{\infty} \Psi_{r,m}{}^* \frac{-k^2}{2\omega\varepsilon(k^2 - \alpha_{nm}{}^2)^{1/2}} \Psi_{p,m} \right] = -A_n \Psi_{r,0}{}^*, \tag{21}$$

where index r varies in the same interval as index p. Thus the linear system involves the same number of equations as unknowns and can readily be solved for the unknowns F_{np} that lead to the calculation of the spectral coefficients B_{nm} and C_{nm} of the diffracted field in the half-spaces I and II, respectively, through a substitution in Eqs. (11), (16), and (19).

3. NUMERICAL APPLICATIONS

Numerical results are presented in the form of equiamplitude contours of the diffracted electric-field intensity within the xOz plane. This method of presentation lucidly demonstrates how the incident Gaussian beam is affected by the periodic planar screen. Furthermore, far-field radiation patterns are evaluated that are found to be very important from an engineering point of view.

The plane-wave representation of the Gaussian beam is obtained by approximating the integral in Eq. (6) with a Gaussian quadrature scheme, as described below. We can define a relative error for this approximation by introducing a fine grid of N_p points. This grid extends $8w_0$ along the transverse x' direction of the incident Gaussian beam and $3w_0$ along the longitudinal z' direction. The relative error is defined through

$$\text{error} = \frac{1}{N_p} \sum_1^{N_p} \frac{|\tilde{E}_{y'}^{\text{inc}} - E_{y'}^{\text{inc}}|^2}{|E_{y'}^{\text{inc}}|^2}, \tag{22}$$

where $\tilde{E}_{y'}^{\text{inc}}$ denotes the approximate summation of relation (7) and $E_{y'}^{\text{inc}}$ refers to the exact Gaussian beam of Eq. (1). Such a 2D error definition for the one-dimensional expansion in relation (7) ensures that the influence of both the deviation from the paraxial regime inherent in Eq. (1) as well as the neglect of the evanescent waves in Eq. (6) can be measured sufficiently well in the case of small kw_0 or near the $z' = 0$ plane, respectively.

It can be inferred from Fig. 2 that in all cases a reasonable accuracy (≤8%) can be obtained by incorporating less than 100 plane waves combined in a Gaussian quadrature scheme, as outlined below. It should be noticed that better accuracy is achieved for larger values of kw_0 with a parallel increase of the number of EPW's required for convergence. This is expected because larger kw_0 values result in narrower and more peaked spectra.

In what follows, the Gaussian beam is expressed as a superposition of 90 elementary plane waves, giving a maximum error in amplitude equal to 0.1% and a maximum error of 1° in phase. This level of accuracy is obtained by dividing the $-\pi/2$ to $\pi/2$ interval in Eq. (6) into three regions. The first extends from $-2\pi/9$ to $2\pi/9$ and is subsequently divided into 12 intervals of equal size. In every interval the EPW's are selected by applying the Gaussian integration scheme of fifth order.[15] The second and third regions extend from $-\pi/2$ to $-2\pi/9$ and from $2\pi/9$ to $\pi/2$, respectively. Each is divided into three intervals, and the EPW's in every interval are selected by applying the previously mentioned scheme. The diffracted electric-field intensity from each elementary plane wave is expanded in terms of 31 ($m = -15$ to 15) Floquet harmonics. The maximum value of index m should be large enough to incorporate all propagating Floquet harmonics and at least 5 to 6 times as many evanescent modes. The higher-order waveguide mode used in the expansion of the surface current corresponds to $P = 12$. The above-mentioned upper

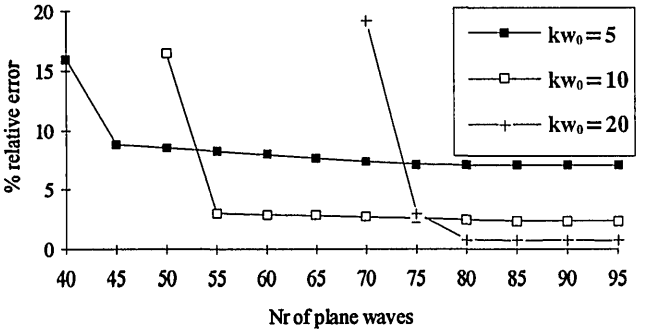

Fig. 2. Relative error versus number (Nr) of plane waves. The grid consists of $N_p = 1250$ points.

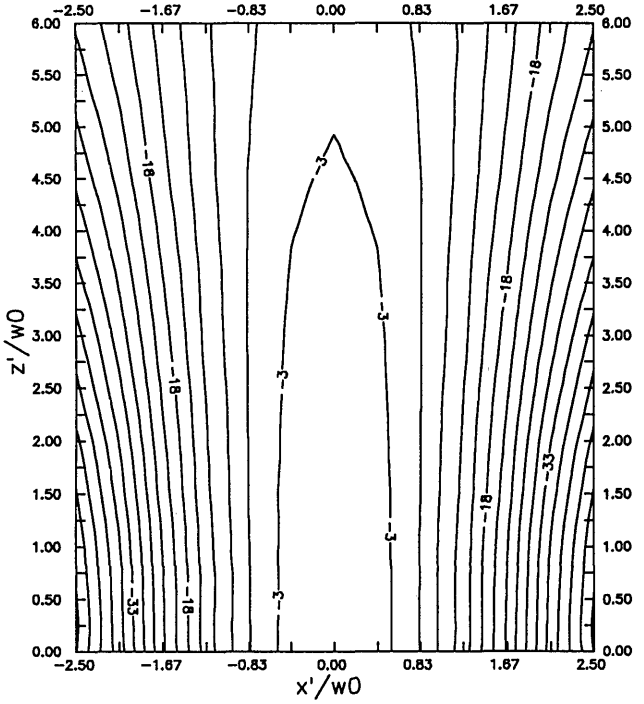

Fig. 3. Equiamplitude contour map of the exact Gaussian beam.

limits of summation ensure an accurate solution for the combinations of wavelength and geometric characteristics considered. An energy balance check for each individual incident plane wave (i.e., the normalized difference between the power impinging on the screen and the power diffracted along all directions by the corresponding propagating Floquet harmonics) is performed. The resulting error is found to be extremely small.

In the case of oblique incidence, only the EPW's that hit on the planar surface give rise to a diffracted field that is expanded in terms of Floquet harmonics. The contribution of the rest is found by simply superimposing them to the produced diffracted electric field.

To evaluate the results of the examples to follow, the equiamplitude contours of the exact Gaussian beam, as obtained from Eq. (1), are presented in Fig. 3. Therefore Fig. 3 serves as reference. The intensity levels in all figures are expressed in decibels. Furthermore, a 3-dB spacing between adjacent contour lines has been used. The axis numbering is normalized with respect to the beam's spot size, w_0.

In Figs. 4–8 the product of the wave-number times the beam's spot size, kw_0, satisfies the inequality $kw_0 > 10.0$ corresponding to wide-angle beams. This is by no means a critical restriction and can be relaxed by properly selecting the number and placement of the plane waves that represent the incident beam, as noted in the remarks referring to Fig. 2.

The influence of parameter γ, where $\gamma = a/L_x$, is investigated in Figs. 4. Normal incidence of the Gaussian beam has been assumed ($\varphi_{inc} = 0$). The incident beam has a displacement $d_z = 0$ along the z axis and $d_x = a/2$ along the x axis, thus impinging on the center of a metal strip. The other parameters are fixed to $kL_x = 6.0$ and $w_0/L_x = 1.667$. Figure 4(a) corresponds to the case $\gamma = 0.9$ and, as one expects, the screen behaves closely as a perfectly conducting screen. The diffracted field in region I ($z > 0$) very nearly approximates the exact Gaussian beam that corresponds to a totally reflected beam from a perfectly

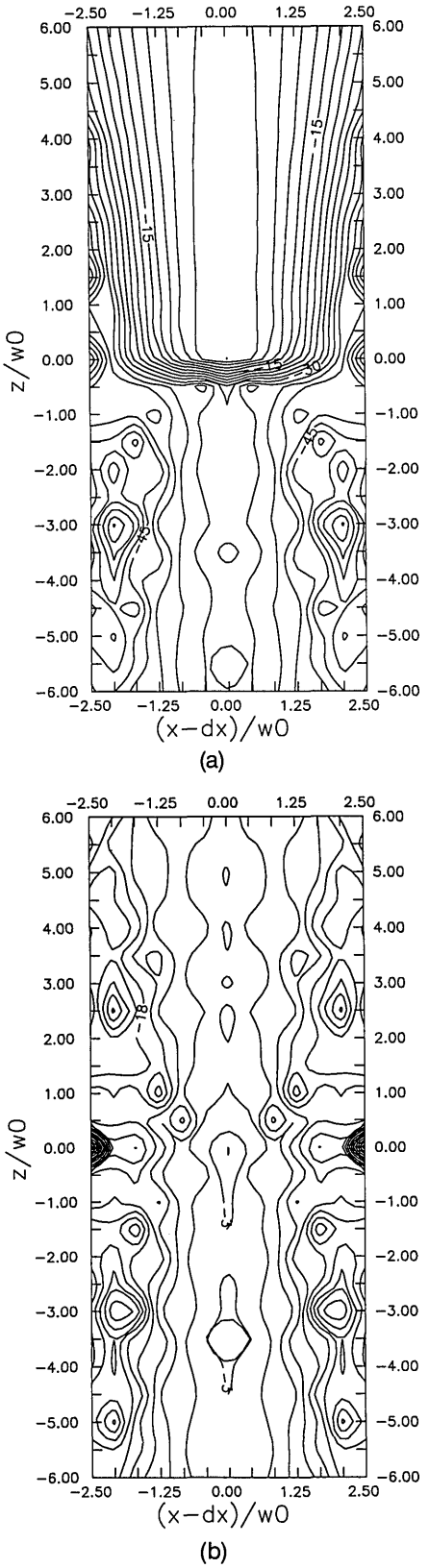

Fig. 4. Equiamplitude contour map of the diffracted electric-field intensity. $\varphi_{inc} = 0°$, $d_z = 0$, $d_x = a/2$, $kL_x = 6.0$, $w_0/L_x = 1.6667$. (a) $\gamma = 0.9$, (b) $\gamma = 0.5$.

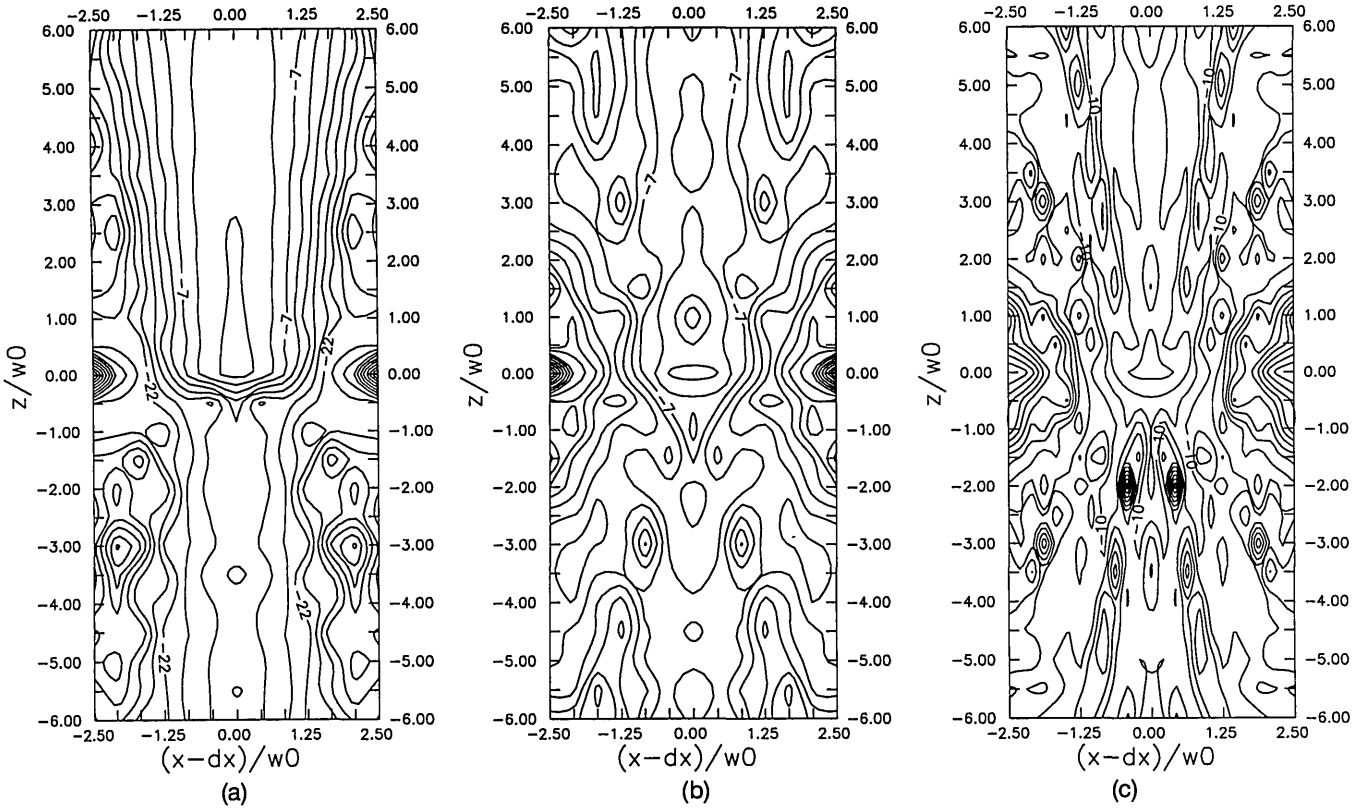

Fig. 5. Equiamplitude contour map of the diffracted electric-field intensity: $\varphi_{inc} = 0°$, $d_z = 0$, $d_x = a/2$, $\gamma = 0.75$, $w_0/L_x = 1.6667$. (a) $kL_x = 6.0$, (b) $kL_x = 12.0$, (c) $kL_x = 18.0$.

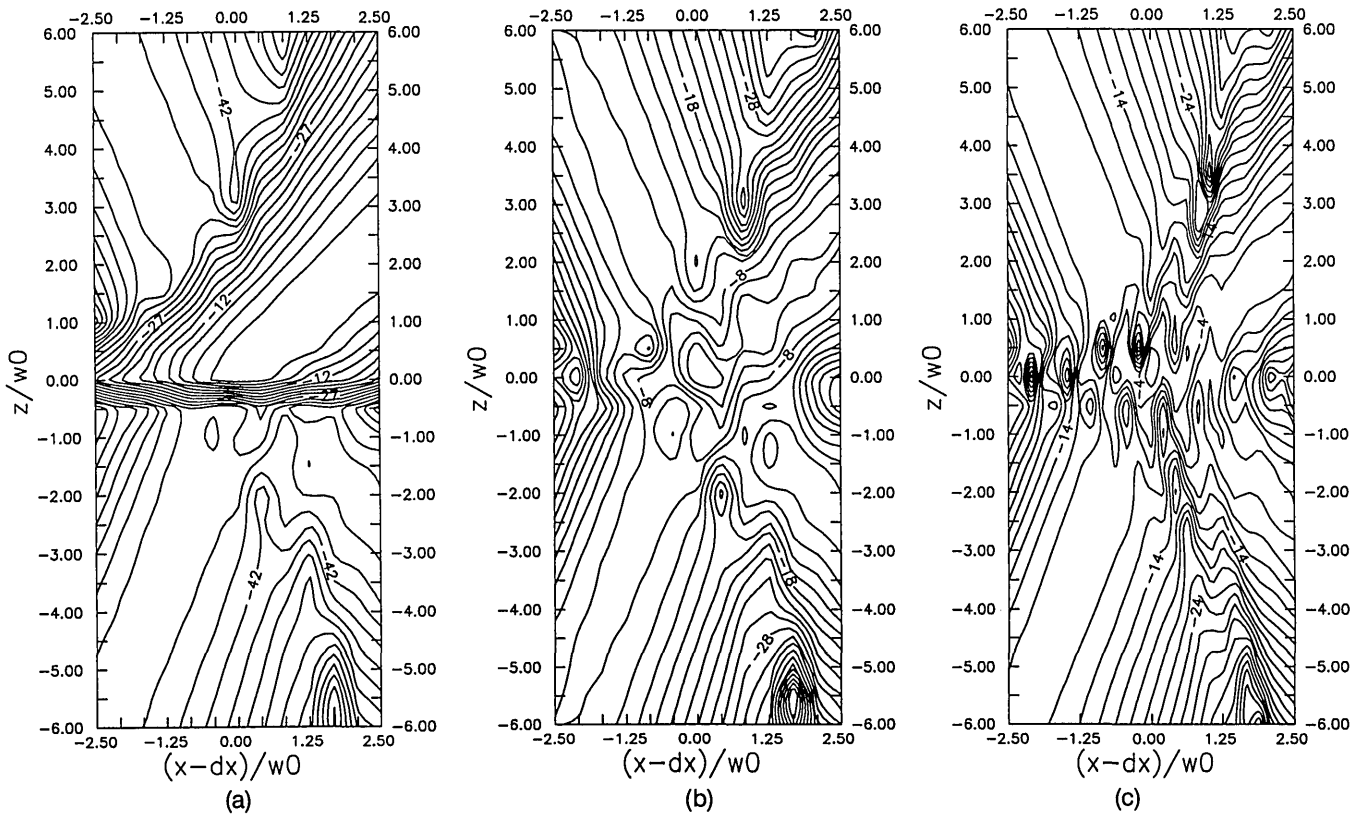

Fig. 6. Equiamplitude contour map of the diffracted electric-field intensity: $\varphi_{inc} = 45°$, $d_z = 0$, $d_x = a/2$, $kL_x = 6.0$, $w_0/L_x = 1.6667$. (a) $\gamma = 0.9$, (b)$\gamma = 0.5$, (c) $\gamma = 0.3$.

conducting metal sheet. The transmitted field in region II ($z < 0$) is at least 20 dB lower than the field in region I. In Fig. 4(b) parameter γ is set to $\gamma = 0.5$. This results in a weak pattern in region I, whereas a significant portion of the incident radiation is transmitted into region II. The equiamplitudes in regions I and II are distorted as compared with those in Fig. 3. Yet the reflected and transmitted beams can be clearly observed.

The effect of the wavelength is considered in Fig. 5 for the case of normal incidence. Parameter γ is held constant ($\gamma = 0.75$), $w_0/L_x = 1.667$, $d_z = 0$, and $d_x = a/2$. In Fig. 5(a) it is assumed that $kL_x = 6.0$. The pattern in region I resembles in a considerable degree the exact Gaussian beam. Reducing the wavelength in Fig. 5(b), where $kL_x = 12.0$, causes the incident radiation to penetrate deeper in region II, whereas the contour patterns are totally distorted. In Fig. 5(c) $kL_x = 18.0$ and the phenomena already noticed in Fig. 5(b) are amplified.

The case of oblique incidence for different values of aspect ratios is presented in Figs. 6, in which $\varphi_{\text{inc}} = 45°$, $d_z = 0$, $d_x = a/2$, $kL_x = 6$, and $w_0/L_x = 1.667$. Figure 6(a) corresponds to $\gamma = 0.9$, Fig. 6(b) corresponds to $\gamma = 0.5$, and Fig. 6(c) corresponds to $\gamma = 0.3$. The comments made above for Figs. 4(a) and 4(b) are also valid for Figs. 6(a)–6(c). A qualitative explanation of the equiamplitude contours found in Figs. 6(a)–6(c) can be given with the aid of theory. Suppose that the incident beam, in a rough approximation, is represented only by a plane wave having a wave vector lying along the direction of propagation of the beam. For the combination of parameters considered, only the two lower-order Floquet harmonics corresponding to $m = -1$ and $m = 0$ (specular term) will propagate in region I, and subsequently only the two lower-order Floquet harmonics $m = -1$, $m = 0$ (forward term) will propagate in region II. Therefore, in this rough approximation, the incident plane wave will give rise to two plane waves in region I (the propagating Floquet harmonics $m = -1, 0$) and two plane waves in region II ($m = -1, 0$). Returning to our approach, and taking into account the fact that the beam is decomposed into a set of elementary plane waves having their wave vectors around the axis of the incident beam, one should expect that the diffracted beam will be composed of mainly four distinct beams. This effect is readily identified in Figs. 6(a)–6(c).

The far-field pattern is evaluated through the electric field produced at distance $\mathbf{r}$ by a surface field distribution as given by[16]

$$E_y^s(\mathbf{r}) = \int_{\text{screen}} \frac{\exp(-jkR)}{2\pi R}\left(jk + \frac{1}{R}\right)\frac{z}{R}E_y(\mathbf{r}')\mathrm{d}s', \qquad \mathbf{r}' + \mathbf{R} = \mathbf{r}. \quad (23)$$

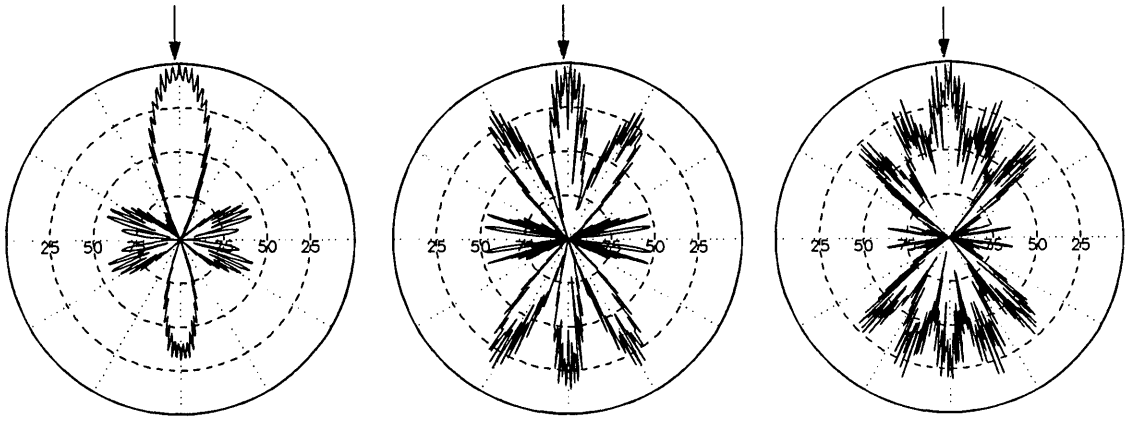

Fig. 7. Far-field radiation patterns. Parameters are set as in Figs. 5.

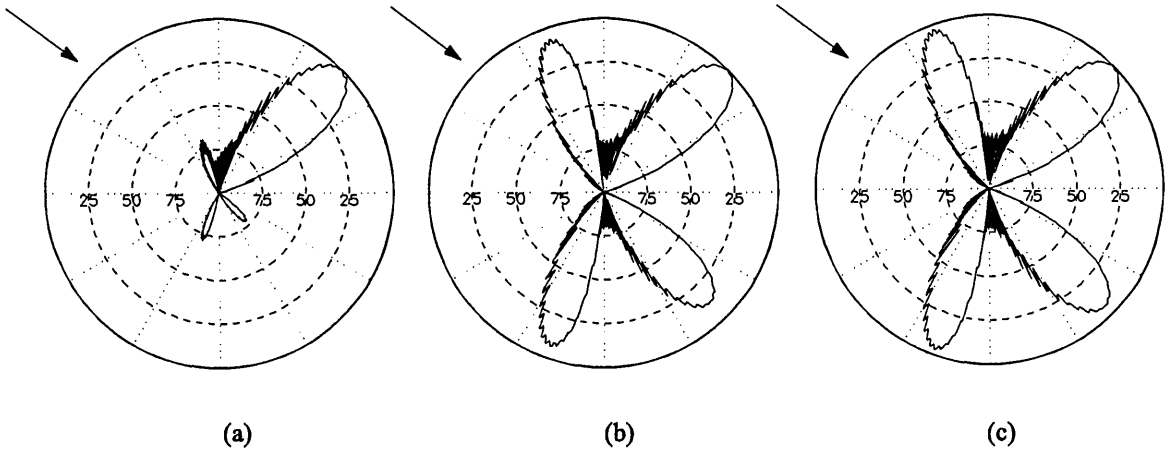

Fig. 8. Far-field radiation patterns. Parameters are set as in Figs. 6.

The integration is carried out numerically over a sufficiently large number of periods, ensuring that the surface field distribution outside this interval has dropped below an appropriately small level. The interval of integration is divided into a number of subintervals, and an eighth-order Gaussian integration is applied to each one.

The corresponding far-field radiation patterns of Figs. 5 and 6 are given in Figs. 7 and 8. The qualitative behavior of the screen has already been outlined through the discussion of the near-field contour maps. The polar diagrams offer a closer identification of the generated subbeams in addition to the quantitative measure of the individual strength of each subbeam.

4. CONCLUSIONS

The diffraction of a 2D Gaussian-profile beam from a periodic planar screen of perfectly conducting strips has been examined. The incident beam is decomposed into an elementary plane-wave spectrum. The diffraction of each EPW is determined with the aid of the spectral domain method, which relates the diffracted electric field to the induced surface current on the metallic portions of the screen. Finally, the spectral coefficients of the unknown surface-current density are involved in a linear system that is obtained by the method of moments.

The equiamplitude contour maps that have been presented in Section 3 verify the fact that this periodic planar screen can find numerous potential applications in beam shaping and frequency filtering. The numerical results are very sensitive to the variation of the parameter γ and to the wavelength λ, and they exhibit the desired behavior in the limiting cases (i.e., $\gamma = 0.9$ and $L_x/\lambda < 1$). For specific combinations of wavelength and geometric characteristics, the equiamplitude contours of the diffracted beam strongly resemble those of the exact Gaussian beam. Moreover the mechanism of subbeam generation in the diffracted electric-field intensity pattern is clearly explained. This evidence is strongly supported by further presentation of far-field polar radiation patterns.

The analysis presented above is readily extendable to 2D periodic planar screens as well as to higher-order Gaussian beam modes.

REFERENCES

1. T. K. Gaylord and M. G. Moharam, "Analysis and applications of optical diffraction by gratings," Proc. IEEE **73,** 894–937 (1985).
2. C. C. Chen, "Scattering by a two-dimensional periodic array of conducting plates," IEEE Trans. Antennas Propag. **AP-18,** 660–665 (1970).
3. K. Kobayashi and T. Inoue, "Diffraction of a plane wave by an inclined parallel plate grating," IEEE Trans. Antennas Propag. **36,** 1424–1434 (1988).
4. R. Petit and G. Tayeb, "Theoretical and numerical study of gratings consisting of periodic arrays of thin and lossy strips," J. Opt. Soc. Am. A **7,** 1686–1692 (1990).
5. R. S. Chu and T. Tamir, "Bragg diffraction of Gaussian beams by periodically modulated media," J. Opt. Soc. Am. **66,** 220–226 (1976).
6. R. S. Chu and T. Tamir, "Diffraction of Gaussian beams by periodically modulated media for incidence angles close to Bragg angle," J. Opt. Soc. Am. **66,** 1348–1440 (1976).
7. R. S. Chu, J. A. Kong, and T. Tamir, "Diffraction of Gaussian beams by a periodically modulated layer," J. Opt. Soc. Am. **67,** 1555–1561 (1977).
8. M. G. Moharam, T. K. Gaylord, and R. Magnusson, "Bragg diffraction of finite beams by thick gratings," J. Opt. Soc. Am. **70,** 300–304 (1980).
9. T. Kojima, "Diffraction of Hermite–Gaussian beams from sinusoidal conducting gratings," J. Opt. Soc. Am. A **7,** 1740–1744 (1990).
10. S. Zhang and T. Tamir, "Spatial modifications of Gaussian beams diffracted by reflection grating," J. Opt. Soc. Am. A **6,** 1368–1381 (1989).
11. A. Yariv, *Optical Electronics* (Saunders, Philadelphia, Pa., 1991), Chap. 2.
12. E. M. Khaled, S. C. Hill, and P. W. Barber, "Scattered/internal intensity for dielectric object with Gaussian beam illlumination," in *Proceedings of the Eighth Annual Review of Progress in Applied Computational Electromagnetics* (U.S. Naval Postgraduate School, Monterey, Calif., 1992), pp. 82–89.
13. E. E. Kriezis, D. P. Chrissoulidis, and A. G. Papagiannakis, *Electromagnetics and Optics* (World Scientific, Singapore, 1992), Chap. 9.
14. G. Scott, *The Spectral Domain Method in Electromagnetics* (Artech, Boston, Mass., 1989), Chaps. 1 and 2.
15. M. Abramowitz and I. A. Stegun, *Handbook of Mathematical Functions* (Dover, New York, 1972), Chap. 25.
16. A. Ishimaru, *Electromagnetic Wave Propagation, Radiation and Scattering* (Prentice-Hall, Englewood Cliffs, N.J., 1991), Chap. 6.